IEEE Access
Multidisciplinary | Rapid Review | Open Access Journal

Received February 17, 2019, accepted March 6, 2019, date of publication March 11, 2019, date of current version April 1, 2019.

*Digital Object Identifier 10.1109/ACCESS.2019.2904144*

# Determination of Local Voltage Control Strategy of Distributed Generators in Active Distribution Networks Based on Kriging Metamodel

**PENG LI[1], (Member, IEEE), CHUANCHI ZHANG[1], XIAOPENG FU[1], (Member, IEEE), GUANYU SONG[1], (Member, IEEE), CHENGSHAN WANG[1], (Senior Member, IEEE), AND JIANZHONG WU[2], (Member, IEEE)**

[1]Key Laboratory of Smart Grid of Ministry of Education, Tianjin University, Tianjin 300072, China
[2]School of Engineering, Institute of Energy, Cardiff University, Cardiff CF24 3AA, U.K.

Corresponding author: Xiaopeng Fu (fuxiaopeng@tju.edu.cn)

This work was supported by the National Natural Science Foundation of China under Grant U1866207 and Grant 51807132.

**ABSTRACT** The increasing penetration of uncontrollable distributed generators (NDGs) exacerbates the risk of voltage violations in active distribution networks (ADNs). It is difficult for a centralized control strategy to meet the requirements of fast voltage and reactive power control because of the heavy computational and communication burdens. Local voltage control based on real-time measurements can respond quickly to the frequent fluctuations of distributed generators (DGs). In this paper, a local voltage control strategy of DGs with reactive power optimization based on a kriging metamodel is proposed. First, to build the metamodel for local voltage control, the steps for determining the input variables are presented in detail, and the effects of different variables on the accuracy of the metamodel are analyzed. Then, taking minimum network losses and voltage deviations as the objective function, we construct the metamodel for local voltage control based on kriging methods. Finally, operation strategies for DGs are developed by calculating the optimally weighted vector based on real-time measurements, and the operation strategies for DGs will be added into the original sample set to improve the accuracy of the metamodel. The proposed local voltage control strategy based on only the local measurements can quickly respond to the frequent DG fluctuations, reduce the communication burden for large networks and improve the adaptability of local voltage control in ADNs. Case studies under different scenarios on the IEEE 33-node system and the IEEE 123-node system are conducted to verify the effectiveness of the proposed method, and the results show that the proposed method can effectively solve the problems of voltage deviation and voltage fluctuation caused by the high penetration of DGs.

**INDEX TERMS** Active distribution networks (ADNs), distributed generator (DG), local voltage control, metamodel.

## I. INTRODUCTION

In recent years, the increasing number of distributed generators (DGs) integrated into electrical distribution systems [1], [2] has brought significant changes in both the construction and operation of distribution networks to transform from passive to active distribution networks (ADNs) [3]. The integration of numerous DGs in distribution networks has many benefits, such as decreased system losses, improved reliability of the power supply and reduced environmental pollution [4]. However, the problems of voltage violation [5] and voltage fluctuation are exacerbated in ADNs due to the presence of the uncontrollable distributed generators (NDGs), such as photovoltaic (PV) and wind turbine (WT) [6], making operation of ADNs relatively complex and challenging [7], [8].

Voltage control is an effective means of ensuring the rate of qualified voltage and reducing network losses. The main voltage control methods are the centralized control method, distributed method and local control method. The centralized control method must collect measurement information on the entire network and allocate controllable resources to

The associate editor coordinating the review of this manuscript and approving it for publication was Salvatore Favuzza.

achieve global optimization of the system [9]. However, with increasing DG penetration, it is difficult for the traditional centralized control methods to adapt to the distribution network because of the limitations of traditional dispatching methods, such as the large scale of communication information and the high cost of investment [10], [11]. Besides, centralized control strategy usually need to collect and process the measurement information of the whole system [12], however, many customers will prefer not to share their private information in real-time with a central control unit [13], and the parameters of grids, and sometimes even the topology of the grid, are only partially known [14], [15], which also make it difficult for centralized control methods to adapt to ADNs. The distributed method [16], [17] holds promise for addressing these issues of the centralized method by improving the voltage regulation capability and reducing the investment cost through coordination among nodes [18]. However, this method also requires communication among the controllers in each area, and many are required iterations to obtain an acceptable optimal solution [19], thus inspiring the local control method. Compared with the centralized control method and distributed method, the local control strategy based only on local measurements has significant advantages of non-communication, high computation efficiency and strong reliability [20] and can provide a fast response to the frequent fluctuations of DGs [21]. The local voltage control method is suitable for supplying real-time power adjustment of DG inverters [22].

Different local voltage control strategies for DGs have been widely proposed, including supplying reactive power compensation [23] and providing active power curtailment [24] based on local voltage measurements, adjusting the power factor based on the active power output of DGs [21], or a combination of these strategies [25]. The Italian LV CEI 0-21 [26] and German's BDEW MV guideline [27] presented the $Q-V$ curve, where the reactive power is defined by local voltage measurements. Considering the potential for accommodating the increased capacities of DGs in ADNs, the optimal power flow has been used to compare the local control with the centralized control [20]. A local voltage control strategy based on the $Q-V$ curve was proposed [23] where the reactive power compensation and active power curtailment of DGs are adjusted based on local measurements to solve the problem of voltage violation. To solve the problem of overvoltage caused by the high penetration of DGs, the use of droop-based active power curtailment methods has been proposed [28]. The $P-Q$ standard curve has been used to determine the amount of local reactive compensation based on the voltage sensitivity matrix and quasi static analysis [29]. In addition, a centralized parameter tuning model of control curves has been built to determine the local voltage control strategies for DGs [30], where the $Q-V$ and $P^{\text{curt}}-V$ curves of DG inverters are mathematically formulated based on piecewise linearization.

The reactive power compensation of DGs can be adjusted based on local measurements using the local control curves in these control strategies. However, these control strategies have complex solution processes, and their performance depends on the tuning of the control parameters. To lighten the computational burden with large networks and reduce the dependence of control strategies on parameters, a local voltage control strategy based on kriging metamodel is proposed in this paper. A metamodel between the local measurements and the reactive power outputs of DGs is built using an intelligent algorithm through continuous learning and training. The method proposed in this paper can determine the control strategies of DG inverters by calculating the optimal weighted vector based on real-time measurements, thereby achieving the goal of reducing system losses and improving the voltage profile.

The metamodel is a modelling method that replaces the complex calculation model in the analysis and optimization process. The introduction of the metamodel can reduce the difficulty of the optimization problem. Various metamodel techniques are widely used in the engineering field, including the quadratic response surface, radial basis function, kriging model, multivariate adaptive regression splines, and support vector regression model [31]. Based on its accurate predictions of highly nonlinear or irregular behaviors, the kriging model is selected to build the metamodel in this paper. The major contributions of this paper are as follows.

1) To build a metamodel for local voltage control, the steps for determining the input variables are presented in detail, and the effects of different control variables on the accuracy of the metamodel are analyzed.

2) Taking minimum network losses and voltage deviations of ADNs as the objective function, we build a metamodel between the local measurements and the reactive power output of DGs based on the kriging metamodel to realize local voltage control of ADNs.

The remainder of the paper is organized as follows. Section II presents the method for building the metamodel for local voltage control based on the selection of control variables and establishment of the metamodel. The method for solving the local voltage control strategy is presented in Section III. Case studies are presented in Section IV to illustrate the effectiveness of the proposed method using the modified IEEE 33-node system and IEEE 123-node system. Finally, conclusions are drawn in Section V.

## II. BUILDING OF A METAMODEL FOR LOCAL VOLTAGE CONTROL

In this section, the method for building the metamodel for local voltage control is presented in terms of the selection of control variables and the establishment of the metamodel.

### A. KRIGING METAMODEL

The kriging metamodel is an interpolation method based on statistical theory. It consists of a regression model and a non-parametric stochastic process [32]. For the set of sample points $\boldsymbol{X} = [\boldsymbol{x}_1, \boldsymbol{x}_2, \cdots, \boldsymbol{x}_h, \cdots \boldsymbol{x}_m]^{\mathrm{T}}$ ($\boldsymbol{x}_h$ is a row vector with $n$ elements) and the set of objective functions

$\boldsymbol{Y} = [\boldsymbol{y}_1, \boldsymbol{y}_2, \cdots, \boldsymbol{y}_h, \cdots \boldsymbol{y}_m]^{\mathrm{T}}$ ($\boldsymbol{y}_h$ is a row vector with $q$ elements), the kriging metamodel can be expressed as follows:

$$\boldsymbol{Y} = \boldsymbol{f}^{\mathrm{T}}\boldsymbol{\beta} + z(\boldsymbol{X}) \tag{1}$$

where $\boldsymbol{f}$ is the basis function matrix with order $p \times m$ and $\boldsymbol{\beta}$ is the coefficient matrix with order $p \times q$. $p$ is the order of the regression model. The commonly used basis functions are the constant function, linear function, and quadratic function. Since the choice of the basis function has little effect on the accuracy of the metamodel, the constant function is selected as the basis function of the regression model in this paper, i.e., $p = 1, \boldsymbol{f}|_{1\times m} = [1, 1, \cdots, 1]$. $z(\boldsymbol{X})$ is a random process with zero mean and variance $\sigma^2$.

### B. SELECTION OF CONTROL VARIABLES

The effects of multiple different variables on the design target are often considered because of the complex design object in the engineering problem. Therefore, the effects of different control variables on the accuracy of the metamodel are considered in this paper. The accuracy of the kriging metamodel is related to the variance $\sigma^2$: a smaller $\sigma^2$ corresponds to higher accuracy of the metamodel. The control variables are selected in the following process [33].

*Step 1:* Select control variables from local measurements.

*Step 2:* Build metamodels based on the sample data, where $\Delta Q_h^{\mathrm{NDG}}$ is used as the output variable, and the control variables selected in Step 1 are used as the input variables.

*Step 3:* Calculate the variances of the metamodels built in Step 2.

*Step 4:* Sort the variances by value in increasing order.

*Step 5:* Build the metamodels using different numbers of control variables, where the control variables are individually added into the input variables following the order of Step 4.

*Step 6:* Calculate the variances of the metamodels built in Step 5.

*Step 7:* Determine the number of input variables according to the trend of variances obtained in Step 6.

In this paper, the control variables are selected from local voltage measurements and local power measurements. In addition, since the loads of the same area are strongly related to time, the control variables are also selected around time. Twelve variables are considered the input variables to build the metamodel for local voltage control: $t_h$, $U_{h-2}^{\mathrm{NDG}}$, $U_{h-1}^{\mathrm{NDG}}$, $w$, $d_m$, $\Delta U_{h-1}^{\mathrm{NDG}}$, $Q_{h-2}^{\mathrm{NDG}}$, $Q_{h-1}^{\mathrm{NDG}}$, $\Delta Q_{h-1}^{\mathrm{NDG}}$, $P_h^{\mathrm{NDG}}$, $P_{h-1}^{\mathrm{NDG}}$ and $\Delta P_h^{\mathrm{NDG}}$.

### C. METAMODEL FOR LOCAL VOLTAGE CONTROL

#### 1) OBJECTIVE FUNCTION

To simultaneously consider the economic efficiency and voltage profile of ADNs, this paper takes the minimum network losses and voltage deviations of ADNs as the objective function [34].

$$f = \min\left\{\sum_{t=1}^{T}\left[\omega_1 \sum_{ij\in\Omega_{\mathrm{b}}} R_{ij}\left(I_{t,ij}\right)^2 + \omega_2 \sum_{i=1}^{N_N}\left|U_{t,i}^2 - 1\right|\right]\right\} \tag{2}$$

The metamodel for local voltage control is built based on model (1). $\boldsymbol{Y} = [\Delta Q_1^{\mathrm{NDG}}, \Delta Q_2^{\mathrm{NDG}}, \cdots, \Delta Q_h^{\mathrm{NDG}}, \cdots, \Delta Q_m^{\mathrm{NDG}}]^{\mathrm{T}}$ is the output and is a column vector composed of the reactive power variation of DG. $m$ is the number of samples used to build the metamodel for local voltage control. $\boldsymbol{X} = [\boldsymbol{x}_1, \boldsymbol{x}_2, \cdots, \boldsymbol{x}_h, \cdots \boldsymbol{x}_m]^{\mathrm{T}}$ is the input matrix, which is composed of historical data of local measurements. $\boldsymbol{x}_h$ is a row vector composed of the control variables selected in the last part.

The voltage variables and power variables should satisfy the following constraints.

#### 2) SYSTEM POWER FLOW CONSTRAINTS

The DistFlow branch model is used to model the distribution network [35]. It is mathematically described by the following constraints:

$$\sum\nolimits_{ik\in\Omega_{\mathrm{b}}} P_{t,ik} = \sum\nolimits_{ji\in\Omega_{\mathrm{b}}}\left(P_{t,ji} - R_{ji}I_{t,ji}^2\right) + P_{t,i} \tag{3}$$

$$\sum\nolimits_{ik\in\Omega_{\mathrm{b}}} Q_{t,ik} = \sum\nolimits_{ji\in\Omega_{\mathrm{b}}}\left(Q_{t,ji} - X_{ji}I_{t,ji}^2\right) + Q_{t,i} \tag{4}$$

$$U_{t,j}^2 = U_{t,i}^2 - 2\left(R_{ij}P_{t,ij} + X_{ij}Q_{t,ij}\right) + \left(R_{ij}^2 + X_{ij}^2\right)I_{t,ji}^2 \tag{5}$$

$$P_{t,i} = P_{t,i}^{\mathrm{NDG}} - P_{t,i}^{\mathrm{L}} \tag{6}$$

$$Q_{t,i} = Q_{t,i}^{\mathrm{NDG}} - Q_{t,i}^{\mathrm{L}} \tag{7}$$

$$I_{t,ij}^2 = \frac{P_{t,ij}^2 + Q_{t,ij}^2}{U_{t,i}^2} \tag{8}$$

Constraints (3) and (4) represent the active and reactive power balance of node $i$ at period $t$. Ohm's law over branch $ij$ at period $t$ is expressed as (5). Constraints (6) and (7) indicate the total active and reactive power injection of node $i$ at period $t$. The current magnitude of each line can be determined by (8)

#### 3) SYSTEM SECURITY CONSTRAINTS

The operation constraints of ADNs are expressed as follows:

$$U_i^{\min} \le U_{t,i} \le U_i^{\max} \tag{9}$$

$$-I_{ij}^{\max} \le I_{t,ij} \le I_{ij}^{\max} \tag{10}$$

#### 4) DG OPERATION CONSTRAINTS

$$P_{t,i}^{\mathrm{NDG}} \le P_{t,i}^{\mathrm{NDG,max}} \tag{11}$$

$$-\frac{P_{t,i}^{\mathrm{NDG}}\sqrt{1-(\kappa_i^{\min})^2}}{\kappa_i^{\min}} \le Q_{t,i}^{\mathrm{NDG}} \le \frac{P_{t,i}^{\mathrm{NDG}}\sqrt{1-(\kappa_i^{\min})^2}}{\kappa_i^{\min}} \tag{12}$$

$$\sqrt{\left(P_{t,i}^{\mathrm{NDG}}\right)^2 + \left(Q_{t,i}^{\mathrm{NDG}}\right)^2} \le S_i^{\mathrm{NDG}} \tag{13}$$

Based on the sample data, a multivariate normal distribution likelihood function defined by parameters $\{\beta, \sigma^2\}$ is built.

$$L\left(\left\{\beta, \sigma^2\right\}|\boldsymbol{Y}\right) = \frac{1}{\sqrt{\left(2\pi\sigma^2\right)^m \det\left[\boldsymbol{R}\left(\boldsymbol{X}\right)\right]}} \times \mathrm{e}^{-\left\{\left(\boldsymbol{Y}-\boldsymbol{f}^{\mathrm{T}}\beta\right)^{\mathrm{T}}\boldsymbol{R}(\boldsymbol{X})^{-1}\left(\boldsymbol{Y}-\boldsymbol{f}^{\mathrm{T}}\beta\right)\right\}/2\sigma^2} \tag{14}$$

where $\det[\boldsymbol{R}(\boldsymbol{X})]$ denotes the determinant of $\boldsymbol{R}(\boldsymbol{X})$. $\boldsymbol{R}(\boldsymbol{X})$ denotes the correlation matrix and can be expressed by

$$\boldsymbol{R}(\boldsymbol{X}) = \begin{bmatrix} \boldsymbol{R}(\boldsymbol{x}_1, \boldsymbol{x}_1) & \cdots & \boldsymbol{R}(\boldsymbol{x}_1, \boldsymbol{x}_m) \\ \vdots & \ddots & \vdots \\ \boldsymbol{R}(\boldsymbol{x}_1, \boldsymbol{x}_m) & \cdots & \boldsymbol{R}(\boldsymbol{x}_m, \boldsymbol{x}_m) \end{bmatrix} \tag{15}$$

The Gaussian function used as the correlation function in this paper can be expressed as follows.

$$R(\boldsymbol{x}_l, \boldsymbol{x}_h) = \prod_{\mu=1}^{n_\theta} \mathrm{e}^{-\theta_\mu d_\mu^2} \tag{16}$$

where $n_\theta$ is the number of input variables used to build the metamodel. $\theta_\mu$ is the unknown correlation parameters used to fit the metamodel. $d_\mu = \boldsymbol{x}_{h_\mu} - \boldsymbol{x}_{l_\mu}$ denotes the distance between $\boldsymbol{x}_{h_\mu}$ and $\boldsymbol{x}_{l_\mu}$, where $\boldsymbol{x}_{h_\mu}$ and $\boldsymbol{x}_{l_\mu}$ are the $\mu$th components of sample points $\boldsymbol{x}_h$ and $\boldsymbol{x}_l$.

$\beta$ and $\sigma^2$ can be obtained by using the weighted least squares method and the maximum likelihood estimation, respectively:

$$\beta = \left(\boldsymbol{f}\boldsymbol{R}(\boldsymbol{X})^{-1}\boldsymbol{f}^{\mathrm{T}}\right)^{-1}\boldsymbol{f}\boldsymbol{R}(\boldsymbol{X})^{-1}\boldsymbol{Y} \tag{17}$$

$$\sigma^2 = \frac{1}{m}\left(\boldsymbol{Y} - \boldsymbol{f}^{\mathrm{T}}\beta\right)^{\mathrm{T}}\boldsymbol{R}(\boldsymbol{X})^{-1}\left(\boldsymbol{Y} - \boldsymbol{f}^{\mathrm{T}}\beta\right) \tag{18}$$

The estimated values of $\beta$ and $\sigma^2$ are related to the correlation parameter $\boldsymbol{\theta}$, where $\boldsymbol{\theta} = \left[\theta_1, \theta_2, \cdots, \theta_{n_\theta}\right]$. An unconstrained optimization model can be obtained by maximum likelihood estimation based on the likelihood function (14).

$$\min\left\{\det[\boldsymbol{R}(\boldsymbol{X})]^{\frac{1}{m}}\sigma^2\right\} \tag{19}$$

The correlation function parameters are determined by solving the above optimization model. Then, the estimated values of $\beta$ and $\sigma^2$ can be obtained.

## III. APPLICATION OF THE LOCAL VOLTAGE CONTROL STRATEGY OF DGS

In this section, the local voltage control strategy of DGs can be obtained by calculating the optimal weighted vector based on local measurements, which can help to reduce the network losses and improve the voltage profile.

Based on the metamodel in Section II, $\Delta Q_{t^*}^{\mathrm{NDG}}$ is given by:

$$\Delta Q_{t^*}^{\mathrm{NDG}} = \beta + z\left(\boldsymbol{x}^*\right) \tag{20}$$

where $\Delta Q_{t^*}^{\mathrm{NDG}}$ is the reactive power output of the DG between sampling times $t^*$ and $t^* - 1$ and $\boldsymbol{x}^*$ is the row vector composed of control variables at $t^*$.

$\Delta Q_{t^*}^{\mathrm{NDG}}$ can also be expressed by the column vector composed of the reactive power variation of the DG:

$$\Delta Q_{t^*}^{\mathrm{NDG}} = \boldsymbol{c}^{\mathrm{T}}\boldsymbol{Y} \tag{21}$$

where $\boldsymbol{c}$ is the weighted coefficient vector.

Due to the unbiased constraints, the mean-square error (MSE) of equations (20) and (21) should be minimized, and the expectation of difference between (20) and (21) must be zero:

$$\begin{cases} \min\langle \mathrm{E}[(\boldsymbol{c}^{\mathrm{T}}\boldsymbol{Y})^2 - \{\beta + z(\boldsymbol{x}^*\}^2]\rangle \\ \mathrm{E}\left[\boldsymbol{c}^{\mathrm{T}}\boldsymbol{Y} - \{\beta + z\left(\boldsymbol{x}^*\right)\}\right] = 0 \end{cases} \tag{22}$$

The weighted optimal coefficient vector $\boldsymbol{c}$ is obtained by calculating the optimization model (22). Then, the reactive power variation of the DG between $t^*$ and $t^* - 1$ is obtained.

$$\Delta Q_{t^*}^{\mathrm{NDG}} = \beta + \boldsymbol{r}\left(\boldsymbol{x}^*, \boldsymbol{X}\right)^{\mathrm{T}}\boldsymbol{R}(\boldsymbol{X})^{-1}\left(\boldsymbol{Y} - \boldsymbol{f}^{\mathrm{T}}\beta\right) \tag{23}$$

where $\boldsymbol{r}(\boldsymbol{x}^*, \boldsymbol{X})$ is the correlation vector between $\boldsymbol{x}^*$ and $\boldsymbol{X}$:

$$\boldsymbol{r}\left(\boldsymbol{x}^*, \boldsymbol{X}\right) = \left[R\left(\boldsymbol{x}_1, \boldsymbol{x}^*\right), R\left(\boldsymbol{x}_2, \boldsymbol{x}^*\right), \cdots, R\left(\boldsymbol{x}_m, \boldsymbol{x}^*\right)\right]^{\mathrm{T}} \tag{24}$$

The operation strategy of the DG at $t^*$ can be expressed by:

$$Q_{t^*}^{\mathrm{NDG}} = \beta + \boldsymbol{r}\left(\boldsymbol{x}^*, \boldsymbol{X}\right)^{\mathrm{T}}\boldsymbol{R}(\boldsymbol{X})^{-1}\left(\boldsymbol{Y} - \boldsymbol{f}^{\mathrm{T}}\beta\right) + Q_{t^*-1}^{\mathrm{NDG}} \tag{25}$$

In the control strategy proposed in this paper, the accuracy of the metamodel is critical and determines the performance of the control strategy. In the optimization process, the objective function and constraints are calculated based on the initial metamodel. Therefore, after the operation strategies of the DGs at $t^*$ are determined, the control strategies of DGs at $t^*$ will be added to the original sample set, and the metamodel will be updated accordingly to improve its accuracy. The schematic of the local voltage control strategy of DGs in ADNs based on the kriging metamodel is shown in Fig. 1.

**TABLE 1. Basic installation parameters of DGs.**

| Number | Type | Node | Capacity/kVA |
|---|---|---|---|
| 1 | PV | 9 | 1200 |
| 2 | WT | 18 | 1500 |
| 3 | PV | 27 | 1200 |
| 4 | WT | 33 | 1500 |

## IV. CASE STUDIES AND ANALYSIS

In this section, the effectiveness of the proposed local voltage control strategy is verified on the modified IEEE 33-node system [36] and IEEE 123-node system [37]. The numerical experiments were conducted on a computer with an Intel (R) Core (TM) i5-3470 CPU running at 3.70 GHz with 8 GB of RAM.

### A. MODIFIED IEEE 33-NODE SYSTEM

The IEEE 33-node system includes 37 lines with a voltage level of 12.66 kV. The base power is 1.0 MW. The total active power and reactive power demands are 3715 kW and 2300 kVAr, respectively. The test case is shown in Fig. 2.

To fully consider the impact of high penetration of DG integration on power losses and voltage deviation, two PVs and two WTs are integrated into the networks. It is assumed that the capacity is equal to the rated real power of DGs.

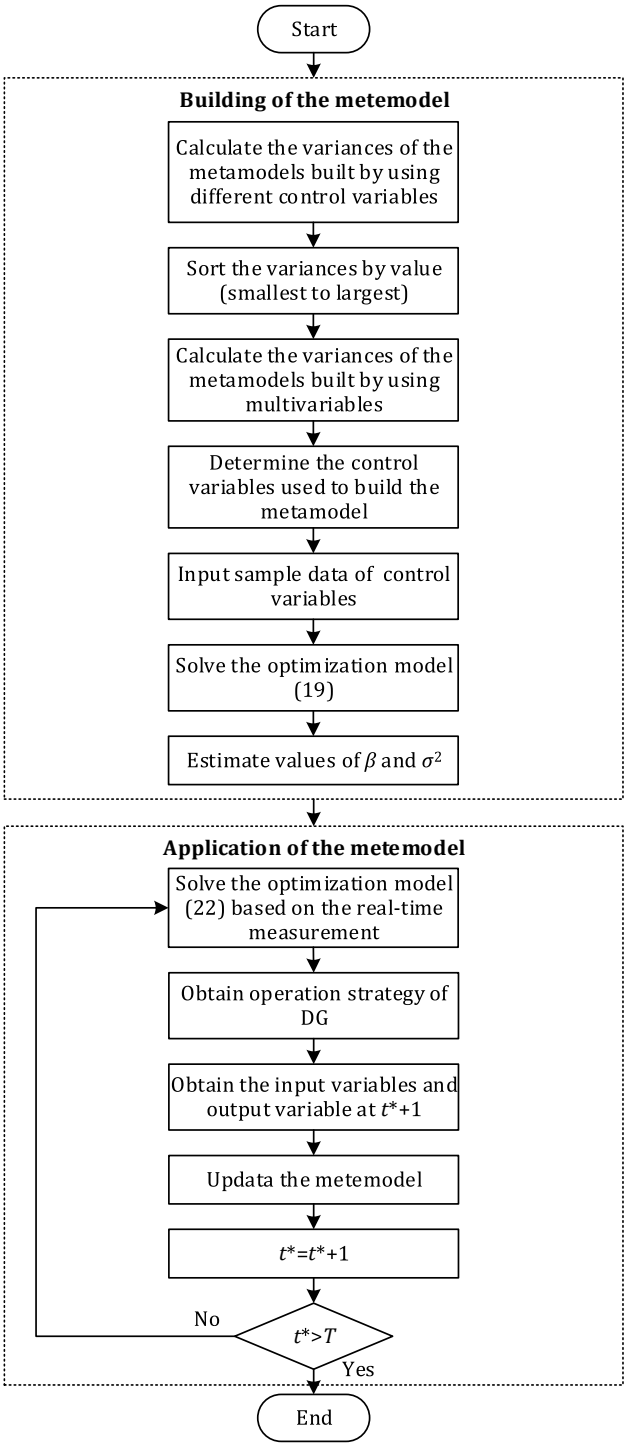


**FIGURE 1.** Schematic of the proposed control strategy.

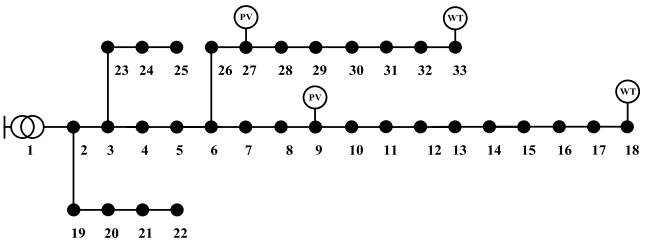


**FIGURE 2.** Structure of the modified IEEE 33-node system.

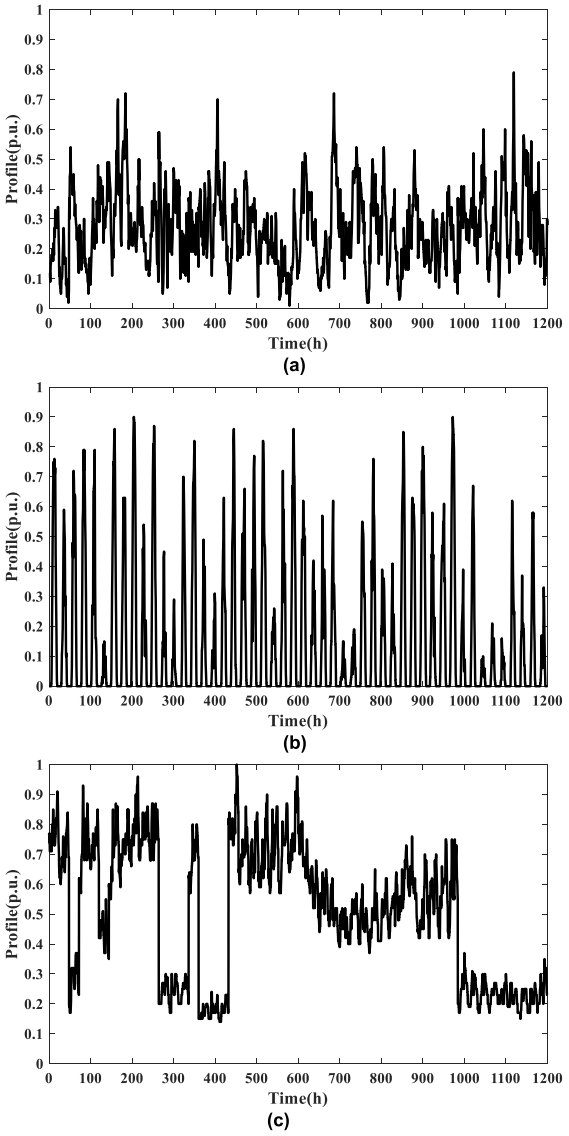


**FIGURE 3.** Annual operation curves. (a) Operation curves of WT. (b) Operation curves of PV. (c) Curves of the load.

The basic installation parameters are presented in Table 1. The weight coefficients $\omega_1$ and $\omega_2$ are set at 0.83 and 0.17 by the analytic hierarchy process (AHP) [38]. The lower and upper bounds of the system voltage are set to 0.95 p.u. and 1.05 p.u., respectively.

### 1) METAMODEL FOR LOCAL VOLTAGE CONTROL

To obtain accurate local measurements, the historical operation data are selected to generate data used to build the metamodel. The operation curves of the load, PV and WT are presented in Fig. 3.

The DACE toolbox [39] is used to build the metamodel in MATLAB. The metamodel for local voltage control is built for each DG based on the sample data. The first step is to calculate the variances of the metamodels, which are built by using the different control variables described in

**TABLE 2. Variances under different control variables.**

| Variables | $\sigma_9^2(\times 10^8)$ | $\sigma_{18}^2(\times 10^8)$ | $\sigma_{27}^2(\times 10^8)$ | $\sigma_{33}^2(\times 10^8)$ |
|---|---|---|---|---|
| $t_h$ | 1.1266 | 1.1077 | 0.9831 | 1.2637 |
| $U_{h-2}^{\mathrm{NDG}}$ | 1.4171 | 1.1222 | 1.4459 | 1.2798 |
| $U_{h-1}^{\mathrm{NDG}}$ | 1.4788 | 1.1402 | 1.4804 | 1.2905 |
| $w$ | 1.5394 | 1.1513 | 1.5105 | 1.2952 |
| $d_m$ | 1.5308 | 1.1493 | 1.4932 | 1.2927 |
| $\Delta U_{h-1}^{\mathrm{NDG}}$ | 1.2145 | 1.0062 | 1.1151 | 1.1368 |
| $Q_{h-2}^{\mathrm{NDG}}$ | 1.4151 | 1.1163 | 1.4412 | 1.2656 |
| $Q_{h-1}^{\mathrm{NDG}}$ | 1.5021 | 1.1398 | 1.4836 | 1.2854 |
| $\Delta Q_{h-1}^{\mathrm{NDG}}$ | 0.8109 | 0.9111 | 0.5547 | 1.0054 |
| $P_h^{\mathrm{NDG}}$ | 1.5044 | 1.1428 | 1.4840 | 1.2846 |
| $P_{h-1}^{\mathrm{NDG}}$ | 1.5231 | 1.1433 | 1.4879 | 1.2874 |
| $\Delta P_h^{\mathrm{NDG}}$ | 1.1722 | 0.8066 | 0.4626 | 0.5706 |

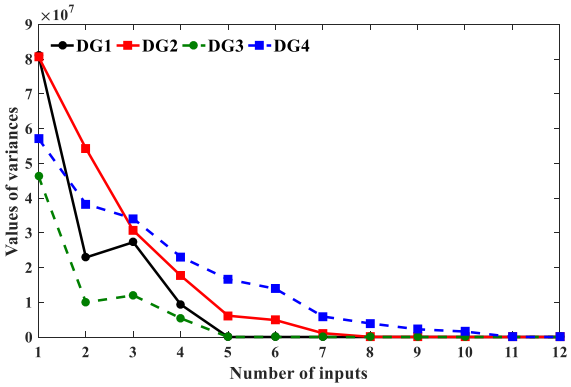


**FIGURE 4. Relationship between the variance and the number of input variable in modified IEEE 33-node system.**

Section II. The values of the variances under the different control variables are shown in Table 2.

The second step is to determine the best number of input variables to achieve the highest accuracy. Fig. 4 shows the relationship between the variances and the number of input variables in modified IEEE 33-node system.

As shown in Fig. 4, the accuracy of the metamodel increases with the number of input variables. Starting at 5 input variables, variances of metamodel of DG1 and DG3 remain unchanged. As the number of input variables increases, more time is consumed, and the computing resources increase. Therefore, $\Delta U_{h-1}^{\mathrm{NDG}}$, $\Delta P_h^{\mathrm{NDG}}$, $t_h$, $\Delta Q_{h-1}^{\mathrm{NDG}}$ and $Q_{h-1}^{\mathrm{NDG}}$ are selected as the input variables to build the metamodel for DG1 and DG3. Until the last variable is added into the input variables, variances of metamodel of DG2 and DG4 tend to 0. Thus, all of the variables shown in Table 2 are selected as the input variables to build the metamodels for DG2 and DG4.

After the input variables are determined, the metamodel for local voltage control is built for each DG. The parameters of the metamodel at nodes 9, 18, 27 and 33 are shown in Table 3.

**TABLE 3. Parameters of the metamodel at nodes 9, 18, 27 and 33.**

| Node | $\beta$ | $\sigma^2$ | $\boldsymbol{\theta}$ |
|---|---|---|---|
| 9 | -0.4819 | 0.0096 | [0.2209, 0.0521, 100, 0.0115, 100] |
| 18 | 0.0437 | 0.0316 | [0.6248, 0.4070, 0.2651, 5.7897, 5.9073, 8.4976, 0.0818, 0.0569, 25.2938, 37.0667, 78.0169, 100] |
| 27 | -0.1038 | 0.0010 | [0.1768, 0.0521, 100, 0.0115, 100] |
| 33 | 0.0383 | 0.0001 | [0.7071, 0.3202, 0.2155, 3.8068, 0.8620, 2.8284, 9.2810, 12.4813, 0.0200, 0.0244, 0.0363, 9.2810] |

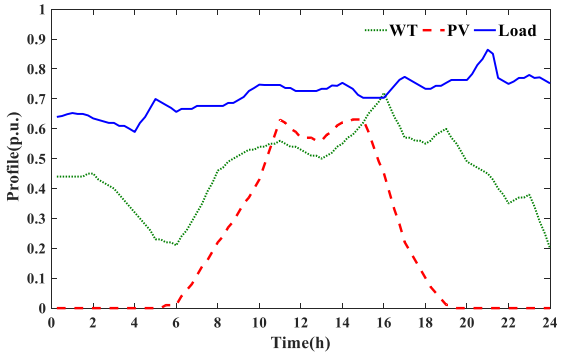


**FIGURE 5. Daily operation curve of DGs and loads.**

**TABLE 4. Optimization results for the three scenarios.**

| Optimization results | Scenario I | Scenario II | Scenario III |
|---|---|---|---|
| Network losses(MW•h) | 1.3805 | 0.3146 | 0.3178 |
| Maximum voltage of ADN (p.u.) | 1.0485 | 1.0083 | 1.0083 |
| Minimum voltage of ADN(p.u.) | 0.9870 | 0.9867 | 0.9867 |

### 2) RESULTS ANALYSIS

By locally controlling the reactive power and outputs of DGs, the proposed strategy is expected to effectively mitigate voltage fluctuation and reduce power losses. Time period between 8h and 16h is selected to verify that the proposed control strategy can effectively solve the problems of voltage deviation and voltage fluctuation caused by the high penetration of DGs. Taking 15 minutes as the time period, the operation curves of the DGs and loads are presented in Fig. 5. Three scenarios are adopted to verify the effectiveness of the proposed control strategy in ADNs.

*Scenario I:* No control strategy is conducted for the DGs.

*Scenario II:* The centralized control strategy based on second-order cone programming [38] is conducted for the DGs.

*Scenario III:* The proposed local control strategy is conducted for the DGs.

The optimization results for the three scenarios are shown in Table 4. Compared with Scenario I, the proposed control strategy in Scenario III can effectively mitigate the voltage deviation and reduce the power losses of the entire network. The performances of the control strategy proposed in this paper are similar to that of the centralized control

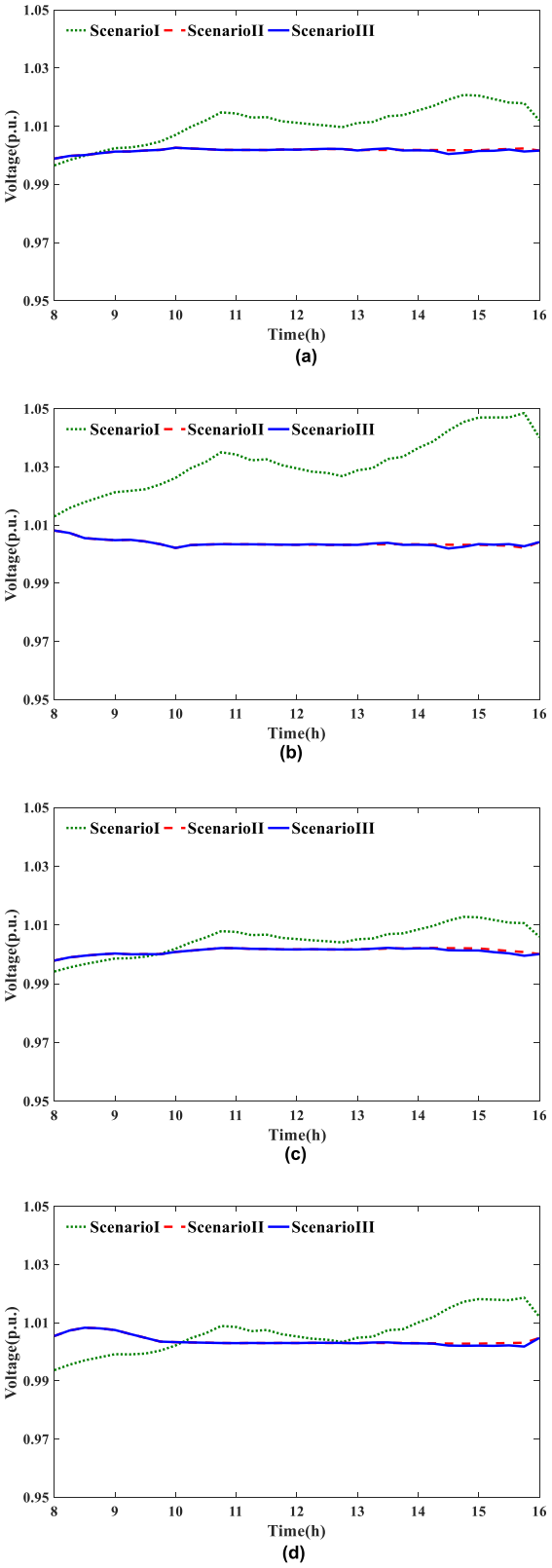


**FIGURE 6.** Voltage profiles at the nodes connecting the DGs in the three scenarios. (a) Voltage profile at node 9. (b) Voltage profile at node 18. (c) Voltage profile at node 27. (d) Voltage profile at node 33.

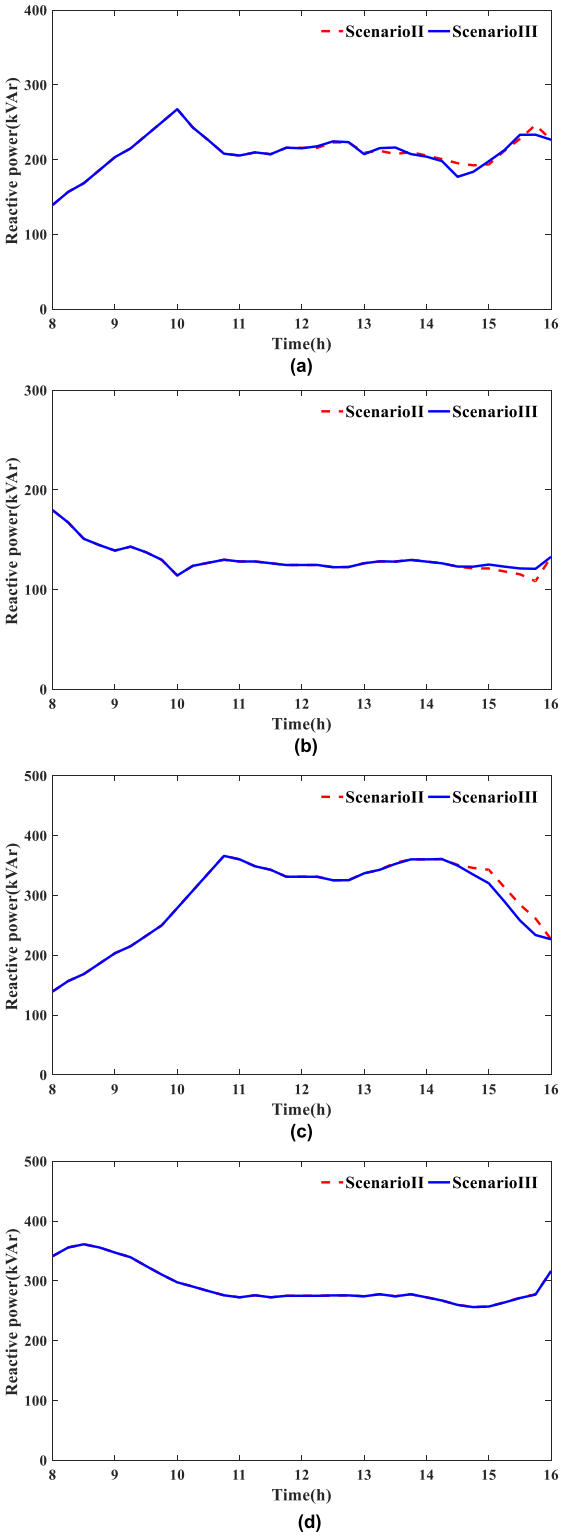


**FIGURE 7.** Operation strategies of the DGs in Scenarios II and III. (a) Reactive power compensation of DG at node 9. (b) Reactive power compensation of DG at node 18. (c) Reactive power compensation of DG at node 27. (d) Reactive power compensation of DG at node 33.

strategy in Scenario II, which has the most optimal use of reactive power of DGs. Because the proposed method is based on less measurement information, it can reduce the computational burden and achieve a nearly globally optimal solution.

**TABLE 5.** Updated variances of the metamodels.

| Node | 9 | 18 | 27 | 33 |
|---|---|---|---|---|
| $\sigma^2$ | 0.0096 | 0.00310 | 0.0010 | 0.0001 |

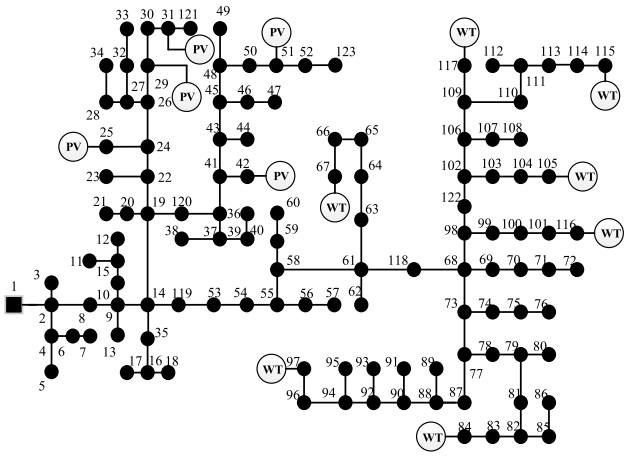

**FIGURE 8.** Structure of the modified IEEE 123-node system.

Fig. 6 shows the voltage profiles at the nodes that connect the DGs in the three scenarios. High penetration of DGs causes frequent voltage fluctuation and severe voltage deviation of the nodes in Scenario I. Node 18 is taken as an example; the high active power outputs of the DGs lead to an obvious increase in the voltage level at $t = 15$. Compared with Scenario I, the voltage profiles are significantly improved in Scenarios II and III. The fluctuation range of the voltage amplitude is controlled at 0.9867-1.0083 in Scenario III. By applying the proposed local voltage control strategy, the DG inverters can adjust the reactive power compensation in real time, which effectively eliminates the voltage fluctuation and reduces the voltage deviation. Although the control strategy proposed in this paper is based only on local measurements, it can effectively reduce the voltage deviation and promote the voltage profile.

Fig. 7 shows the operation strategies of DGs in Scenarios II and III. The results for the two scenarios show that the DGs in Scenarios III and II have basically equal reactive power compensation. In Scenario III, the DG inverters adjust the reactive power in real time based on the local voltage measurements.

Table 5 is the updated variances of metamodels at nodes 9, 18, 27 and 33. Comparing variances of Table 3 and Table 5, it can be seen that since the optimization results are added into the original sample set, the variance of the metamodel at node 18 is reduced, which means the accuracy of the metamodel at node 18 is improved.

### B. MODIFIED IEEE 123-NODE SYSTEM

In this part, a larger scale system of the modified IEEE 123-node system is selected to further verify the effectiveness of the proposed local voltage control strategy. The test case is shown in Fig. 8. The IEEE 123-node system includes 122 lines, and the base power is 1.0 MW. The total active power and reactive power demands are 3490 kW and 1920 kVAr, respectively. Five PVs and seven WTs are integrated into the networks, and the basic installation parameters are presented in Table 6.

**TABLE 6.** Basic installation parameters of DGs.

| Number | Type | Node | Capacity/kVA |
|---|---|---|---|
| 1 | PV | 25 | 500 |
| 2 | PV | 29 | 500 |
| 3 | PV | 31 | 500 |
| 4 | PV | 42 | 500 |
| 5 | PV | 51 | 500 |
| 6 | WT | 67 | 800 |
| 7 | WT | 84 | 800 |
| 8 | WT | 97 | 800 |
| 9 | WT | 105 | 800 |
| 10 | WT | 115 | 800 |
| 11 | WT | 116 | 800 |
| 12 | WT | 117 | 800 |

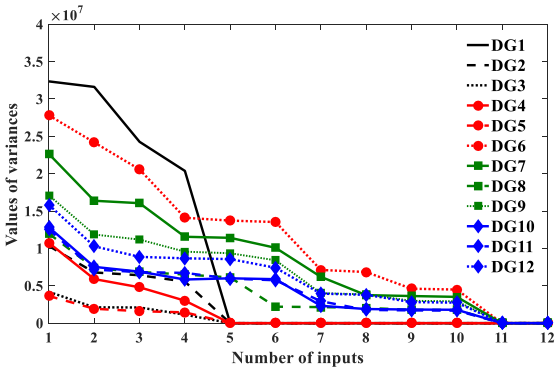


**FIGURE 9.** Relationship between the variance and the number of input variables in modified IEEE 123-node system.

The values of the variances under the different control variables are shown in Table 7. The relationship between the variance and the number of input variables in modified IEEE 123-node system. is shown in Fig. 9. From Fig.9 and Table 7, we can determine that $\Delta U_{h-1}^{\mathrm{NDG}}$, $\Delta P_h^{\mathrm{NDG}}$, $t_h$, $\Delta Q_{h-1}^{\mathrm{NDG}}$ and $Q_{h-2}^{\mathrm{NDG}}$ are selected as the input variables of metamodels at DG1 to DG5, and $\Delta U_{h-1}^{\mathrm{NDG}}$, $U_{h-1}^{\mathrm{NDG}}$, $U_{h-2}^{\mathrm{NDG}}$, $\Delta P_h^{\mathrm{NDG}}$, $P_h^{\mathrm{NDG}}$, $P_{h-1}^{\mathrm{NDG}}$, $\Delta Q_{h-1}^{\mathrm{NDG}}$, $Q_{h-1}^{\mathrm{NDG}}$, $Q_{h-2}^{\mathrm{NDG}}$, $t_h$ and $d_m$ are selected as the input variables of metamodels at DG6 to DG12. The parameters of metamodels are shown in Table 8.

To highlight the performance of the proposed local voltage control strategy in ADNs, $Q - V$ local control strategy [30], where the reactive power is defined by local voltage measurements, is selected as a comparison. Taking the operation curves shown in Fig. 5 as an example again, the optimization

**TABLE 7.** Variances under different control variables.

| Variables | $\sigma^2_{25}$ ($\times 10^7$) | $\sigma^2_{29}$ ($\times 10^7$) | $\sigma^2_{31}$ ($\times 10^7$) | $\sigma^2_{42}$ ($\times 10^7$) | $\sigma^2_{51}$ ($\times 10^7$) | $\sigma^2_{67}$ ($\times 10^7$) | $\sigma^2_{84}$ ($\times 10^7$) | $\sigma^2_{97}$ ($\times 10^7$) | $\sigma^2_{105}$ ($\times 10^7$) | $\sigma^2_{115}$ ($\times 10^7$) | $\sigma^2_{116}$ ($\times 10^7$) | $\sigma^2_{117}$ ($\times 10^7$) |
|---|---|---|---|---|---|---|---|---|---|---|---|---|
| $t_h$ | 1.8109 | 1.8689 | 4.5256 | 1.6496 | 1.6501 | 2.2788 | 2.7357 | 2.7674 | 3.6692 | 3.2162 | 2.6794 | 2.9712 |
| $U^{\mathrm{NDG}}_{h-2}$ | 2.6363 | 2.7191 | 5.1427 | 2.6483 | 2.6303 | 2.2884 | 2.7485 | 2.7820 | 3.6962 | 3.1746 | 2.6832 | 2.9773 |
| $U^{\mathrm{NDG}}_{h-1}$ | 2.6613 | 2.7499 | 5.1665 | 2.6777 | 2.6602 | 2.3033 | 2.7581 | 2.7908 | 3.7093 | 3.2358 | 2.6983 | 2.9953 |
| $w$ | 2.6953 | 2.7853 | 5.1829 | 2.7186 | 2.6996 | 2.3088 | 2.7608 | 2.7965 | 3.7200 | 3.2495 | 2.7010 | 2.9953 |
| $d_m$ | 2.6707 | 2.7591 | 5.1667 | 2.6872 | 2.6686 | 2.3056 | 2.7570 | 2.7925 | 3.7132 | 3.2449 | 2.6978 | 2.9912 |
| $\Delta U^{\mathrm{NDG}}_{h-1}$ | 1.9102 | 1.9445 | 4.5965 | 1.8458 | 1.7924 | 2.0972 | 2.4014 | 2.4309 | 3.3512 | 3.1675 | 2.3858 | 2.7148 |
| $Q^{\mathrm{NDG}}_{h-2}$ | 2.5870 | 2.6843 | 4.6809 | 2.6234 | 2.6052 | 2.2433 | 2.7029 | 2.7389 | 3.6287 | 3.0934 | 2.6309 | 2.9034 |
| $Q^{\mathrm{NDG}}_{h-1}$ | 2.6546 | 2.7452 | 5.0479 | 2.6783 | 2.6588 | 2.2867 | 2.7395 | 2.7761 | 3.6877 | 3.2003 | 2.6773 | 2.9572 |
| $\Delta Q^{\mathrm{NDG}}_{h-1}$ | 1.0235 | 1.2067 | 3.2349 | 0.8942 | 0.9078 | 1.9086 | 2.1930 | 2.2174 | 2.8711 | 2.7802 | 2.2505 | 2.4752 |
| $P^{\mathrm{NDG}}_h$ | 2.6606 | 2.7500 | 5.1073 | 2.6790 | 2.6603 | 2.2999 | 2.7416 | 2.7766 | 3.6873 | 3.2403 | 2.6879 | 2.9856 |
| $P^{\mathrm{NDG}}_{h-1}$ | 2.6653 | 2.7532 | 5.1708 | 2.6782 | 2.6595 | 2.3001 | 2.7480 | 2.7835 | 3.6965 | 3.2407 | 2.6902 | 2.9845 |
| $\Delta P^{\mathrm{NDG}}_h$ | 1.0733 | 1.0318 | 4.7953 | 0.3627 | 0.4188 | 1.5819 | 1.2827 | 1.2524 | 1.1981 | 2.8782 | 1.7106 | 2.2633 |

**TABLE 8.** Parameters of metamodels.

| Node | $\beta$ | $\sigma^2(\times 10^{-5})$ | $\boldsymbol{\theta}$ |
|---|---|---|---|
| 25 | -0.1673 | 2.2853 | [0.6730, 0.5254, 0.0067, 82.0335, 20.4942] |
| 29 | -0.1325 | 2.2866 | [2.0000, 3.8068, 0.0010, 37.1499, 78.0709] |
| 31 | -0.0842 | 20.8535 | [1.2342, 3.2310, 0.0010, 45.5673, 55.7193] |
| 42 | -0.1935 | 1.9599 | [3.9508, 0.3095, 0.0010, 45.5673, 54.6944] |
| 51 | -0.1502 | 1.8543 | [11.8880, 33.6242, 0.9057, 33.6242, 16.8121] |
| 67 | -0.0034 | 2.7039 | [0.9231, 0.5416, 0.3178, 2.9833, 2.0540, 0.1217, 2.8284, 3.3190, 8.9003, 4.3331, 0.0794] |
| 84 | 0.0281 | 3.3477 | [0.3933, 0.1618, 0.0666, 27.9599, 57.1443, 0.0046, 83.2532, 0.0010, 0.7107, 85.5025, 0.0010] |
| 97 | 0.0294 | 3.3897 | [0.7660, 0.3443, 0.2370, 6.1279, 0.9481, 0.0774, 8.0000, 9.3877, 6.8174, 4.0000, 0.0695] |
| 105 | 0.0362 | 3.9351 | [0.7660, 0.3443, 0.2370, 6.1279, 0.9481, 0.0774, 2.7540, 9.3877, 6.8174, 4.0000, 0.0695] |
| 115 | -0.0212 | 4.1334 | [0.4616, 0.1618, 0.0899, 35.6604, 57.1443, 0.0046, 83.2532, 81.4692, 0.0012, 85.5025, 0.0010] |
| 116 | -0.0092 | 3.3233 | [0.7660, 0.8079, 0.2370, 6.1279, 0.9481, 0.0774, 1.0548, 9.3877, 6.8174, 12.9269, 0.0695] |
| 117 | -0.0379 | 4.2048 | [0.7660, 0.3443, 0.2370, 6.1279, 1.3770, 0.0774, 2.7540, 9.3877, 6.8174, 4.9509, 0.0695] |

period is one day. The optimization results of local control curves for DG3 and DG6 are shown in Fig. 10. It can be seen from the Fig.10 that the DG connected at node 67 provides reactive power compensation even the node voltage level reaches 1.03 p.u. The $Q-V$ curve at node 31 does not have dead-zone, which means that $Q-V$ curve becomes 5-point control mode.

Optimization results of the two local control strategies are listed in Table 9. Compared with the $Q-V$ local control strategy, the proposed control strategy effectively mitigates voltage deviation and reduces power losses of the whole network, guaranteeing the secure and economic operation of ADNs.

Fig. 11 shows the minimum voltage of each time period under the two different local control strategies, and the voltage profile under the proposed local control strategy is better than that under the $Q-V$ control strategy.

To verify the robustness of the proposed method under uncertain conditions, Monte Carlo simulations are conducted for the centralized control strategy, the $Q-V$ control

**TABLE 9. Optimization results of the two local control strategies.**

| Optimization results | $Q-V$ control strategy | Proposed local control strategy |
|---|---|---|
| Network losses (MWh) | 0.5904 | 0.4466 |
| Maximum voltage of ADN (p.u.) | 1.0006 | 1.0002 |
| Minimum voltage of AND (p.u.) | 0.9450 | 0.9505 |

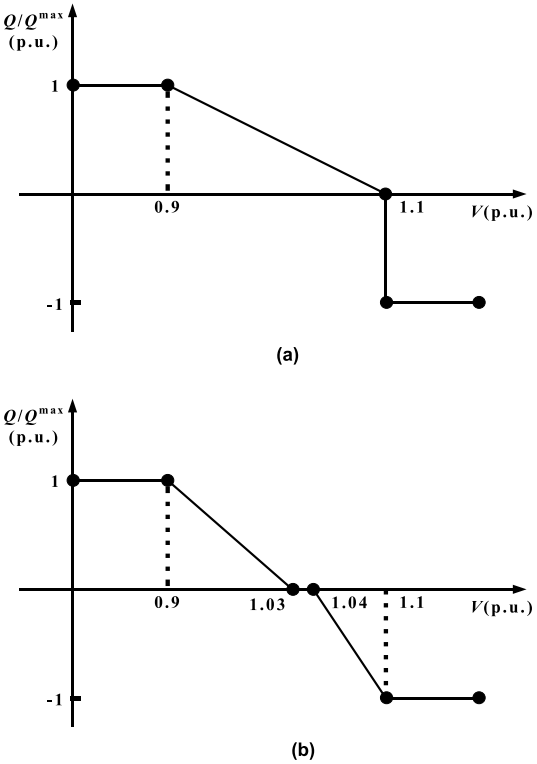


**FIGURE 10.** Local control curves for DG3 and DG6. (a) Local control curve at node31. (b) Local control curve at node 67.

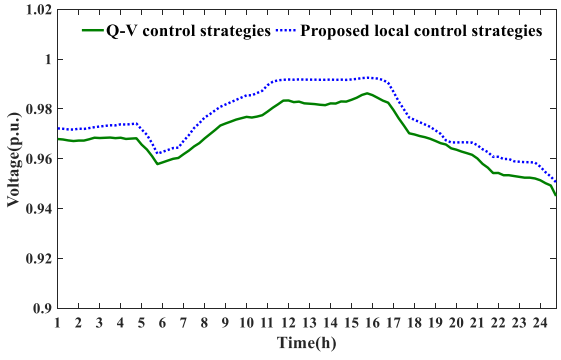


**FIGURE 11.** Minimum voltage of each time period.

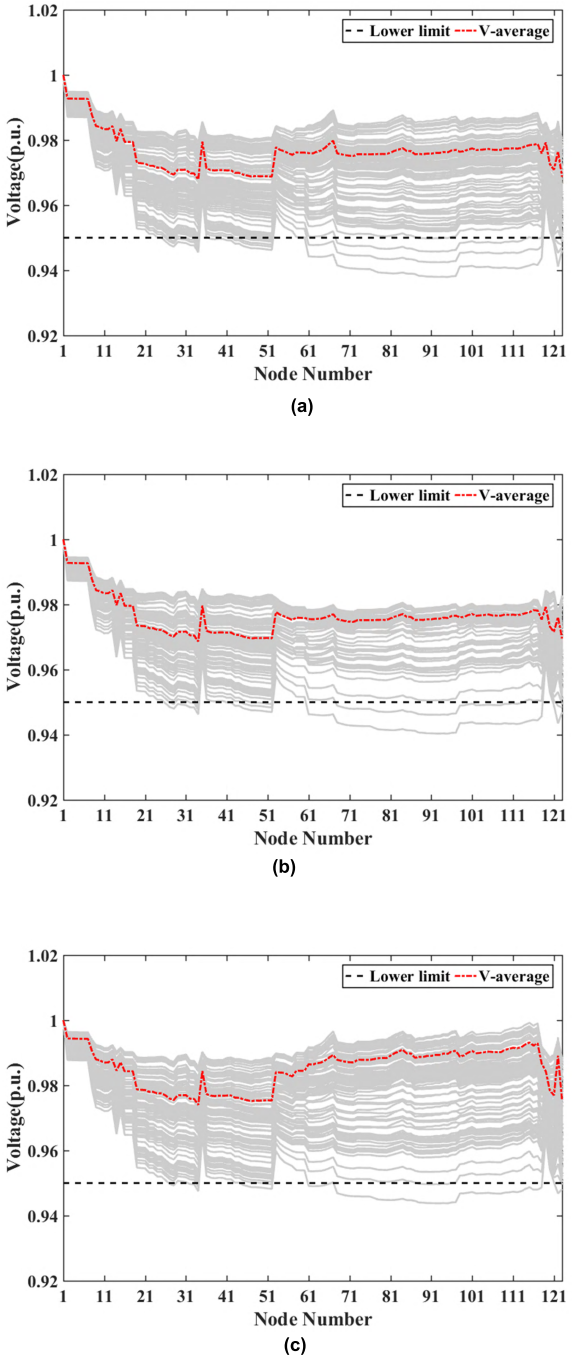


**FIGURE 12.** Voltage distributions of the three control strategies in Monte Carlo simulation. (a) Voltage distributions of the centralized control strategy in Monte Carlo simulation. (b) Voltage distributions of the Q-V control strategy in Monte Carlo simulation. (c) Voltage distributions of the proposed local control strategy in Monte Carlosimulation.

strategy and the proposed local control strategy, in which 500 stochastic scenarios are generated randomly. It is assumed that the actual DG outputs are random variables following normal distributions with ±20% fluctuation ranges.

The voltage distributions in Monte Carlo simulation for the three control strategies are shown in Fig. 12. The red line represents the average voltage distribution, and the grey line is the voltage distribution of the nodes at each optimization period. Test results of the three control strategies in the Monte Carlo simulation are shown in Table 10. Compared to the other two strategies, the problems of voltage violation are less likely to happen for the proposed local control strategy. Considering the uncertainties of DGs, the proposed

**TABLE 10. Test results of the three control strategies in Monte Carlo simulation.**

| Control strategy | Number of secure operation scenarios | Secure operation rate (%) |
|---|---|---|
| Centralized control strategy | 387 | 77.40 |
| $Q-V$ control strategy | 451 | 90.20 |
| Proposed local control strategy | 475 | 95.00 |

control strategies are more robust and can effectively ensure the secure operation of ADNs.

The simulation results demonstrate that the proposed strategy can effectively solve the voltage problem caused by the high penetration of DGs. In conclusion, the proposed local voltage control strategy can quickly respond to the frequent DG fluctuations and effectively reduce the voltage deviation without neither the measurement information of whole system nor the parameters of grids, which is suitable for the local voltage control of large-scale ADNs with high penetration of DGs.

## V. CONCLUSIONS

In this paper, a metamodel-based method to determine the local voltage control strategies for DGs is proposed. To realize the local voltage control of ADNs, a metamodel is built in which different variables are selected as the input variables and the reactive power variation of the DG at the next sampling time is taken as the output. To improve accuracy of the metamodel, the operation strategies for DGs developed by calculating the optimal weighted vector based on real-time measurement will be added into the original sample set. Using only local measurements, the metamodel can be built using the kriging method through training. The proposed method is expected to lighten communication burdens with large network scale and improve the adaptability of local voltage control in ADNs. The tests on the IEEE 33-node system and IEEE 123-node system show that the proposed control strategy significantly improves the voltage profile while reducing network losses. Based on these improvements, the proposed control method has great economic value.

## APPENDIX

### A. SETS

| | |
|---|---|
| $T$ | Set of periods of the controlling time horizon |
| $N_{\mathrm{N}}$ | Set of all nodes |
| $\Omega_{\mathrm{b}}$ | Set of all branches |

### B. INDICES

| | |
|---|---|
| $i, j$ | Indices of nodes |
| $t$ | Indices of time periods |
| $ij$ | Indexes of branches |
| $h$ | Indexes of samples |

### C. VARIABLES

| | |
|---|---|
| $t_h$ | Sampling time of the $h$th sample |
| $U_{h-2}^{\mathrm{NDG}}$ | Voltage of the DG access point at sampling time $t_h-2$ |
| $U_{h-1}^{\mathrm{NDG}}$ | Voltage of the DG access point at sampling time $t_h-1$ |
| $w$ | Sign of weekend; if the day is a weekend, $w=1$; otherwise, $w=0$ |
| $d_m$ | Sampling day in a month |
| $\Delta U_{h-1}^{\mathrm{NDG}}$ | Voltage variation of the DG access point between sampling times $t_h-1$ and $t_h-2$ |
| $Q_{h-2}^{\mathrm{NDG}}$ | Reactive power of the DG at sampling time $t_h-2$ |
| $Q_{h-1}^{\mathrm{NDG}}$ | Reactive power of the DG at sampling time $t_h-1$ |
| $\Delta Q_{h-1}^{\mathrm{NDG}}$ | Reactive power variation of the DG between sampling times $t_h-1$ and $t_h-2$ |
| $P_h^{\mathrm{NDG}}$ | Predicted value of the active power output of the DG at sampling time $t_h$ |
| $P_{h-1}^{\mathrm{NDG}}$ | Active power of the DG at sampling time $t_h-1$ |
| $\Delta P_h^{\mathrm{NDG}}$ | Active power variation of the DG between sampling times $t_h$ and $t_h-1$ |
| $P_{t,ij}$, $Q_{t,ij}$ | Active/reactive power flow of branch $ij$ in period $t$ |
| $P_{t,i}$, $Q_{t,i}$ | Total active/reactive power injection at node $i$ in period $t$ |
| $P_{t,i}^{\mathrm{NDG}}$, $Q_{t,i}^{\mathrm{NDG}}$ | Active/reactive power injection by the NDG at node $i$ in period $t$ |
| $U_{t,i}$ | Voltage magnitude of node $i$ at period $t$ |
| $I_{t,ij}$ | Current magnitude of branch $ij$ at period $t$ |

### D. PARAMETERS

| | |
|---|---|
| $U^{\max}$, $U^{\min}$ | Upper/lower limit of the system voltage |
| $I^{\max}$, $I^{\min}$ | Upper/lower limit of the current magnitude |
| $P_{t,i}^{\mathrm{L}}$, $Q_{t,i}^{\mathrm{L}}$ | Active/reactive power consumption at node $i$ in period $t$ |
| $P_{t,i}^{NDG,max}$ | Upper limit of the active power provided by the NDG at node $i$ in period $t$ |
| $S_i^{NDG}$ | Capacity of the NDG at node $i$ |
| $\kappa_i^{min}$ | Lower limit of the power factor of the NDG at node $i$ |
| $R_{ij}$, $X_{ij}$ | Resistance/reactance of branch $ij$ |
| $\omega_1$, $\omega_2$ | Weight coefficients in the objective function |

## REFERENCES

[1] D. Q. Hung, N. Mithulananthan, and R. C. Bansal, "Integration of PV and BES units in commercial distribution systems considering energy loss and voltage stability," *Appl. Energy*, vol. 113, no. 1, pp. 1162–1170, Jan. 2014.
[2] C. Wang, G. Song, and P. Li, "Optimal siting and sizing of soft open points in active electrical distribution networks," *Appl. Energy*, vol. 189, no. 1, pp. 301–309, Mar. 2017.
[3] J. P. Lopes, N. Hatziargyriou, J. Mutale, P. Djapic, and N. Jenkins, "Integrating distributed generation into electric power systems: A review of drivers, challenges and opportunities," *Electric Power Syst. Res.*, vol. 77, no. 9, pp. 1189–1203, 2007.
[4] A. C. Rueda-Medina and A. Padilha-Feltrin, "Distributed generators as providers of reactive power support—A market approach," *IEEE Trans. Power Syst.*, vol. 28, no. 1, pp. 490–502, Feb. 2013.

[5] M. N. Kabir, Y. Mishra, G. Ledwich, Z. Xu, and R. C. Bansal, "Improving voltage profile of residential distribution systems using rooftop PVs and battery energy storage systems," *Appl. Energy*, vol. 134, no. 1, pp. 290–300, Dec. 2014.

[6] J. Barr and R. Majumder, "Integration of distributed generation in the volt/VAR management system for active distribution networks," *IEEE Trans. Smart Grid*, vol. 6, no. 2, pp. 576–586, Mar. 2015.

[7] H. Ji, C. Wang, P. Li, F. Ding, and J. Wu, "Robust operation of soft open points in active distribution networks with high penetration of photovoltaic integration," *IEEE Trans. Sustain. Energy*, vol. 10, no. 1, pp. 280–289, Jan. 2019.

[8] P. Li *et al.*, "Optimal operation of soft open points in active distribution networks under three-phase unbalanced conditions," *IEEE Trans. Smart Grid*, vol. 10, no. 1, pp. 380–391, Jan. 2019.

[9] J. Zhao, Y. Li, and P. Li, "Local voltage control strategy of active distribution network with PV reactive power optimization," in *Proc. IEEE PES General Meeting*, Jul. 2017, pp. 1–5.

[10] F. Ren, M. Zhang, and D. Sutanto, "A multi-agent solution to distribution system management by considering distributed generators," *IEEE Trans. Power Syst.*, vol. 28, no. 2, pp. 1442–1451, May 2013.

[11] M. E. Elkhatib, R. El-Shatshat, and M. M. A. Salama, "Novel coordinated voltage control for smart distribution networks with DG," *IEEE Trans. Smart Grid*, vol. 2, no. 4, pp. 598–605, Dec. 2011.

[12] M. Kim and S. Bae, "Decentralized control of a scalable photovoltaic (PV)-battery hybrid power system," *Appl. Energy*, vol. 188, pp. 444–455, Feb. 2017.

[13] S. Weckx and J. Driesen, "Optimal local reactive power control by PV inverters," *IEEE Trans. Sustain. Energy*, vol. 7, no. 4, pp. 1624–1633, Oct. 2016.

[14] S. Bolognani and S. Zampieri, "A distributed control strategy for reactive power compensation in smart microgrids," *IEEE Trans. Autom. Control*, vol. 58, no. 11, pp. 2818–2833, Nov. 2013.

[15] S. Bolognani, R. Carli, G. Cavraro, and S. Zampieri, "Distributed reactive power feedback control for voltage regulation and loss minimization," *IEEE Trans. Autom. Control*, vol. 60, no. 4, pp. 966–981, Apr. 2015.

[16] X. Wang, C. Wang, and T. Xu, "Optimal voltage regulation for distribution networks with multi-microgrids," *Appl. Energy*, vol. 201, pp. 1027–1036, Jan. 2018.

[17] W. U. Hongbin, C. Huang, M. Ding, B. Zhao, and P. Li, "Distributed cooperative voltage control based on curve-fitting in active distribution networks," *J. Modern Power Syst. Clean Energy*, vol. 5, no. 5, pp. 777–786, 2017.

[18] Y. Chai, L. Guo, C. Wang, Z. Zhao, X. Du, and J. Pan, "Network partition and voltage coordination control for distribution networks with high penetration of distributed PV units," *IEEE Trans. Power Syst.*, vol. 33, no. 3, pp. 3396–3407, May 2018.

[19] M. Tan, C. Han, X. Zhang, L. Guo, and T. Yu, "Hierarchically correlated equilibrium Q-learning for multi-area decentralized collaborative reactive power optimization," *CSEE J. Power Energy Syst.*, vol. 2, no. 3, pp. 65–72, Sep. 2016.

[20] P. N. Vovos, A. E. Kiprakis, A. R. Wallace, and G. P. Harrison, "Centralized and distributed voltage control: Impact on distributed generation penetration," *IEEE Trans. Power Syst.*, vol. 22, no. 1, pp. 476–483, Feb. 2007.

[21] E. Demirok, P. C. González, K. H. B. Frederiksen, D. Sera, P. Rodriguez, and R. Teodorescu, "Local reactive power control methods for overvoltage prevention of distributed solar inverters in low-voltage grids," *IEEE J. Photovolt.*, vol. 1, no. 2, pp. 174–182, Oct. 2011.

[22] A. Zakariazadeh, O. Homaee, S. Jadid, and P. Siano, "A new approach for real time voltage control using demand response in an automated distribution system," *Appl. Energy*, vol. 117, pp. 157–166, Mar. 2014.

[23] S. Karagiannopoulos, P. Aristidou, and G. Hug, "Hybrid approach for planning and operating active distribution grids," *IET Gener., Transmiss. Distrib.*, vol. 11, no. 3, pp. 685–695, Feb. 2017.

[24] G. Mokhtari, A. Ghosh, G. Nourbakhsh, and G. Ledwich, "Smart robust resources control in LV network to deal with voltage rise issue," *IEEE Trans. Sustain. Energy*, vol. 4, no. 4, pp. 1043–1050, Oct. 2013.

[25] S. Weckx, C. Gonzalez, and J. Driesen, "Combined central and local active and reactive power control of PV inverters," *IEEE Trans. Sustain. Energy*, vol. 5, no. 3, pp. 776–784, Jul. 2014.

[26] *Reference Technical Rules for the Connection of Active and Passive Users to the LV Electrical Utilities*, document CEI 0-21-V1, Dec. 2014.

[27] *Power Generation Systems Connected to the Low Voltage Distribution Network. Technical Minimum Requirements for the Connection to and Parallel Operation With Low Voltage Distribution Networks*, document VDE-AR-N 4105, Aug. 2011.

[28] R. Tonkoski, L. A. C. Lopes, and T. H. M. El-Fouly, "Coordinated active power curtailment of grid connected PV inverters for overvoltage prevention," *IEEE Trans. Sustain. Energy*, vol. 2, no. 2, pp. 139–147, Apr. 2011.

[29] S. Alyami, Y. Wang, C. Wang, J. Zhao, and B. Zhao, "Adaptive real power capping method for fair overvoltage regulation of distribution networks with high penetration of PV systems," *IEEE Trans. Smart Grid*, vol. 5, no. 6, pp. 2729–2738, Nov. 2014.

[30] H. Ji, C. Wang, and P. Li, "A centralized-based method to determine the local voltage control strategies of distributed generator operation in active distribution networks," *Appl. Energy*, vol. 228, pp. 2024–2036, Oct. 2018.

[31] A. Younis and Z. Dong, "Global optimization using mixed surrogates and space elimination in computationally intensive engineering designs," *Int. J. Comput. Methods Eng. Sci. Mech.*, vol. 13, no. 4, pp. 272–289, 2012.

[32] T. W. Simpson, J. Peplinski, P. N. Koch, and J. K. Allen, "Metamodels for computer-based engineering design: Survey and recommendations," *Eng. Comput.*, vol. 17, no. 2, pp. 129–150, Jul. 2001.

[33] G. Henri and N. Lu, "A machine learning approach for real-time battery optimal operation mode prediction and control," in *Proc. IEEE PES Transmiss. Distrib. Conf.*, 2018, pp. 1–9.

[34] M. Nick, R. Cherkaoui, and M. Paolone, "Optimal allocation of dispersed energy storage systems in active distribution networks for energy balance and grid support," *IEEE Trans. Power Syst.*, vol. 29, no. 5, pp. 2300–2310, Sep. 2014.

[35] M. E. Baran and F. F. Wu, "Optimal capacitor placement on radial distribution systems," *IEEE Trans. Power Del.*, vol. 4, no. 1, pp. 725–734, Jan. 1989.

[36] M. E. Baran and F. F. Wu, "Network reconfiguration in distribution systems for loss reduction and load balancing," *IEEE Trans. Power Del.*, vol. 4, no. 2, pp. 1401–1407, Apr. 1989.

[37] W. H. Kersting, "Radial distribution test feeders," *IEEE Trans. Power Syst.*, vol. 6, no. 3, pp. 975–985, Aug. 1991.

[38] J. A. Taylor and F. S. Hover, "Convex models of distribution system reconfiguration," *IEEE Trans. Power Syst.*, vol. 27, no. 3, pp. 1407–1413, Aug. 2012.

[39] S. Lophaven, H. Nielsen, and J. Søndergaard, "DACE—A MATLAB Kriging toolbox," Dept. Inform. Math. Model., Tech. Univ. Denmark, Lyngby, Denmark, Tech. Rep. IMM-REP-2002-12, 2002.


**PENG LI** (M'11) received the B.S. and Ph.D. degrees in electrical engineering from Tianjin University, Tianjin, China, in 2004 and 2010, respectively, where he is currently an Associate Professor with the School of Electrical and Information Engineering.

His current research interests include distributed generation system and microgrid, smart distribution systems, and transient simulation and analysis.

**CHUANCHI ZHANG** received the B.S. degree in electrical engineering from Tianjin University, Tianjin, China, in 2015, where he is currently pursuing the M.S. degree in electrical engineering.

His current research interests include distribution system modelling and optimization.

**XIAOPENG FU** (M'16) received the B.S. and Ph.D. degrees in electrical engineering from Tianjin University, Tianjin, China, in 2011 and 2016, respectively.

His research interests include analysis of distributed generation systems, microgrid, and simulation of electromagnetic transients.

**GUANYU SONG** (M'17) received the B.S. and Ph.D. degrees in electrical engineering from Tianjin University, Tianjin, China, in 2012 and 2017, respectively, where he is currently a Lecturer with the School of Electrical and Information Engineering.

His current research interests include optimal planning and operation of smart distribution systems.

**CHENGSHAN WANG** (SM'11) received the Ph.D. degree in electrical engineering from Tianjin University, Tianjin, China, in 1991.

From 1994 to 1996, he was a Senior Academic Visitor with Cornell University, Ithaca, NY, USA. From 2001 to 2002, he was a Visiting Professor with the Carnegie Mellon University, Pittsburgh, PA, USA. He is currently a Professor with the School of Electrical and Information Engineering, Tianjin University, where he is also the Director of the Key Laboratory of SmartGrid of the Ministry of Education. His current research interests include distribution system analysis and planning, distributed generation system and microgrid, and power system security analysis.

Dr. Wang is an Editorial Board Member of the *Applied Energy* and the *Journal of Modern Power Systems and Clean Energy*.

**JIANZHONG WU** (M'14) received the Ph.D. degree from Tianjin University, Tianjin, China, in 2004.

From 2004 to 2006, he was with Tianjin University, where he is currently an Associate Professor. From 2006 to 2008, he was a Research Fellow with the University of Manchester, Manchester, U.K. He is currently a Professor with the Cardiff School of Engineering, Institute of Energy, London, U.K. His current research interests include energy infrastructure and smart grids.

Dr. Wu is a member of the Institution of Engineering and Technology and the Association for Computing Machinery.